Separation and Purification Technology 372 (2025) 133350

Contents lists available at ScienceDirect

Separation and Purification Technology

journal homepage: www.elsevier.com/locate/seppur

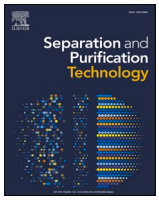

Selective leaching and magnetic separation for efficient recovery of lithium and iron phosphate from Aluminum-Contaminated cathode materials of spent $LiFePO_4$ batteries

Shengxiao Niu [a,b,c], Puwu Liang [b,c,d], Zhicheng Zhang [b], Jinfeng Tang [e,*], Minhua Su [e], Hongli Bao [a,b,c,d,*], Junhua Xu [f,g,*]

[a] College of Chemistry and Materials Science, Fujian Normal University, Fuzhou, Fujian Province 350007, China
[b] Fujian Institute of Research On the Structure of Matter, Chinese Academy of Sciences, Fuzhou, Fujian Province 350002, China
[c] Fujian College, University of Chinese Academy of Sciences, Fuzhou, Fujian Province 350002, China
[d] College of Chemistry, Fuzhou University, Fuzhou, Fujian Province 350108, China
[e] Linköping University - Guangzhou University Research Center On Urban Sustainable Development, School of Environmental Science and Engineering, Guangzhou University, Guangzhou 510006, China
[f] Geological Survey of Finland, P.O. Box 96 FI-02151 Espoo, Finland
[g] PureTech Industry Oy, P.O. Box 55 FI-00740 Helsinki, Finland

ARTICLE INFO

Editor: RAJIV R SRIVASTAVA

Keywords:
$LiFePO_4$
Cathode material powder
Aluminum impurity
Leaching and separation
Magnetic separation

ABSTRACT

The recovery and reuse of resources from spent lithium-ion batteries present significant potential for sustainable development and environmental protection. However, challenges remain, particularly in addressing complex issues such as the removal of aluminum (Al) impurities. This paper introduces an efficient and selective process for leaching lithium (Li) from $LiFePO_4$ cathode material powder, even in the presence of hard-to-remove Al impurities. First, the $LiFePO_4$ cathode material was separated from damaged Al foil current collectors using an environmentally friendly water stripping method, resulting in the active material powder containing Al impurities. In the subsequent process, a small amount of H_3PO_4 was used as a leaching agent, H_2O_2 as an oxidant, and the cathode material was subjected to mechanical activation by ball milling. After continuous optimization of all conditions, an efficient leaching of 99.5 % Li was achieved, with almost all (>99 %) Fe and Al impurities separated as precipitates. Li in the leachate was precipitated as Li_2CO_3 by adding Na_2CO_3 at 95 °C, achieving a purity of 99.2 %. A magnetic separation scheme is presented to successfully separate $FePO_4$ from Al-containing impurities in the leaching residue. After five magnetic separation cycles, the purity of $FePO_4$ exceeded 98.5 %. Additionally, the mechanisms of the entire reaction system were investigated using characterization methods such as laser particle size analysis, XPS, and XRD. A comprehensive economic evaluation of the entire system confirms its feasibility. This eco-friendly selective separation process shows strong potential for industrial applications and makes a valuable contribution to sustainable development.

1. Introduction

Lithium iron phosphate ($LiFePO_4$) batteries, with a high energy density, long lifespan, large capacity, and low self-discharge rate, are crucial for electric vehicles (EVs) and stationary energy storage [1]. The lifespan of $LiFePO_4$ batteries generally ranges from 2000 to 4000 charge–discharge cycles, roughly equivalent to 5 to 10 years [2]. More and more spent batteries will be accumulated over the next five years. Proper storage and disposal of these batteries are crucial, as improper handling can lead to the leakage of organic electrolytes, explosions, and fires [3]. A battery generally consists of components such as the cathode, anode, separator, and electrolyte. $LiFePO_4$ is used as the active material for the cathode in $LiFePO_4$ batteries and contains a rich source of Li and Fe resources. Therefore, recycling spent batteries is an urgent and significant global task, critical for safety, economic value and environmental protection [4].

* Corresponding authors.
E-mail addresses: niushengxiao@fjirsm.ac.cn (S. Niu), liangpuwu@fjirsm.ac.cn (P. Liang), zhangzhicheng@fjirsm.ac.cn (Z. Zhang), Jinfeng@gzhu.edu.cn (J. Tang), mhsu@gzhu.edu.cn (M. Su), hlbao@fjirsm.ac.cn (H. Bao), Junhua.xu@gtk.fi (J. Xu).

https://doi.org/10.1016/j.seppur.2025.133350
Received 26 February 2025; Received in revised form 1 May 2025; Accepted 1 May 2025
Available online 5 May 2025

For the recycling of cathode materials, the most common methods currently include direct regeneration, pyro-metallurgical, and hydro-metallurgical processes. In the direct regeneration method, the LFP cathode material is typically re-lithiated to achieve direct regeneration [5,6]. However, the direct regeneration method struggles to remove metal impurities (Al and Cu) [7], which can affect the lifespan and efficiency of the new battery [8]. Pyrometallurgy involves extracting and recovering metals from materials at high temperatures [9,10]. It generally operates at temperatures above 800 °C, leading to the volatilization of highly reactive Li and the collapse of the $FePO_4$ framework, thereby reducing Li recovery efficiency. Additionally, the high energy consumption of pyrometallurgy significantly increases the cost of recycling, reducing profitability and process sustainability. Hydrometallurgical processes can be conducted at ambient temperature and pressure, offering good metal selectivity and high reaction efficiency, making them more suitable for extracting Li from retired LFP batteries [11,12].

Typical hydrometallurgical methods use various acids as leaching agents, including both organic and inorganic acids [13]. Numerous previous studies have utilized organic acids for leaching cathode materials from waste lithium-ion batteries (LIBs). Li et al. used 0.3 M oxalic acid $H_2C_2O_4$ at 80 °C, achieving a Li leaching rate of 98 % and an Fe leaching rate of 92 % [14]. Yadav et al. achieved a 94 % Li leaching rate and a 95 % Fe leaching rate at room temperature using 4 M methane sulfonic acid CH_3SO_3H [15]. These organic acids not only provide acidity, but also have a certain degree of oxidation, which can achieve a dual effect of acidity and oxidation. Compared to organic acid, inorganic acids, such as the strong acids H_2SO_4 and HCl, are much preferred in the leaching process due to their low cost and high efficiency. Song et al. utilized sulfuric acid [16] for leaching, achieving Li and iron leaching efficiencies of 96.67 % and 93.25 %, respectively, when the liquid–solid (L/S) ratio was 20:1, the sulfuric acid concentration was 2 mol/L, the leaching temperature was 70 °C, and the leaching time was 2 h. Liu et al. employed a hydrochloric acid and sodium hypochlorite [17] leaching system. Under optimal conditions (0.6 mol/L HCl solution, Li:H:ClO = 1.0:1.3:0.6, 20 °C), they achieved a Li leaching rate of over 95 % and an iron leaching rate of less than 0.12 % within just 20 min of reaction time. But inorganic acids usually do not have oxidizing properties, so they often need to be used in combination with other oxidants. Phosphoric acid, as a moderately strong acid, undergoes stepwise ionization in aqueous solution and gradually reaches the ionization equilibrium, which has been employed in the leaching process of LIB cathode materials. Chen et al. demonstrated that over 99 % of Co can be separated and recovered as $Co_3(PO_4)_2$ from waste $LiCoO_2$ cathode materials under the leaching conditions of 40 ℃, 60 min, 4 vol% H_2O_2, 20 mL g^{-1} (L/S) and 0.7 mol/L H_3PO_4[18]. Yang et al. used 0.6 M H_3PO_4 and mechanically activated $LiFePO_4$ for 2 h with EDTA-2Na, maintaining the S/L ratio at 50 g/L. The Li leaching rate reached 94.29 % and the Fe leaching rate reached 97.67 % [19].

Hydrogen peroxide has been widely used as an oxidant in acid leaching processes, because it does not introduce other elements and has a sufficient oxidation potential to meet the requirements [20]. In our laboratory's previous studies, Zhang et al. used an optimized H_2SO_4–H_2O_2 leaching system assisted by a mechanical activation pretreatment, achieving 99 % Li leaching and 0.01 % iron leaching, successfully separating Fe and Li [21]. Moreover, their work also demonstrated the positive effect of mechanical activation (ball milling) before Li leaching, indicating that the particle size of the powder during grinding also has an impact on Li leaching [22]. Normally, in the recycling and separation process, it is difficult to eliminate small Al foil fragments during disassembling, crushing and sieving [23]. Especially, when dealing severely damaged electrodes, it is impossible to completely remove the Al impurities during the pretreatment stage [24]. The presence of Al impurities can compete with the target metals during the leaching and separation process [25]. However, to the best of our knowledge, it is rare to see methods can effectively address the problem of Al impurity in hydrometallurgy technologies. Therefore, developing a green process that can separate Fe and Li in the presence of Al impurities is urgently needed.

In this study, an innovative recycling process was developed to remove Al impurity in harvesting Li and $FePO_4$ from spent LIBs. This work adopted an environmentally friendly water peeling method to separate the cathode material from the Al foil in spent power battery electrode sheets. Phosphoric acid was used as the basic leaching agent with H_2O_2 as the oxidant, with assistance from ball milling pretreatment for mechanical activation. To achieve the optimal process conditions, ball milling pretreatment was performed under various conditions. In addition, the effects of acid concentration, oxidant addition, the solid–liquid ratio, temperature, and stirring speed were thoroughly investigated. Subsequently, the magnetic method was employed to separate Al and $FePO_4$ from the obtained metal residues. Finally, the separation mechanism of Li^+, $FePO_4$, and Al impurities was illustrated.

2. Experimental

2.1. Material and reagents

The $LiFePO_4$ cathode material used in this study was sourced from a local LIB company in China. The 160 Ah power batteries had undergone 800 charge–discharge cycles at a 0.5C rate (80 A) within a voltage range of 2.5 to 4.0 V. After this cycling, the degraded $LiFePO_4$ batteries were employed for the study. The reagents used in this work, including the phosphoric acid (H_3PO_4, 98 %), hydrogen peroxide (H_2O_2, 30 %), sodium carbonate (Na_2CO_3, 99.8 %), and sodium hydroxide (NaOH, 96 %), were all analytical grade reagents purchased from Sinopharm Chemical Reagent Co. and were used without further purification. A neodymium–iron–boron (NdFeB) magnet with a magnetic grade of N35 was used for magnetic separation. All solutions were prepared using deionized water with a resistivity of 18.2 MΩ.

2.2. Instruments and analytical methods

A Planetary Ball Mill (QM-QX1L) was employed for the mechanical grinding of materials. X-ray powder diffraction (XRD) (Rigaku Miniflex 600) with the setting of 40 kV, 40 mA, and Cu − Kα radiation was utilized for crystal structure and phase analysis. An X-ray photoelectron spectroscope (XPS) (Thermo Fisher ESCALAB 250xi) was used for analyzing the valence states of elements in the $LiFePO_4$ and $FePO_4$ samples. Field-emission scanning electron microscopy (FE-SEM) was used to analyze the morphology of the $LiFePO_4$ samples. A micron-level laser particle size analyzer (LS-I3-320) was used to analyze the particle size distribution of the cathode active substances after grinding. Cathode active substances were digested with a microwave digestion system (MWD-500, METASH, Shanghai, China), and elemental analysis was conducted using an inductively coupled plasma optical emission spectrometer (ICP-OES, PerkinElmer Instrument, Avio 200). The quantitative spectral lines used were as follows (wavelength in nm): Li-670.773, Al-396.159, Fe-238.204.

2.3. Treatment of cathode material

An optimized novel water stripping method was used to separate the cathode material powder from the Al foil current collector [22]. Firstly, the electrode sheets of the power battery were cut into 1 cm × 1 cm squares and calcined in air at 450°C for 2 h to remove organic binders such as PVDF and impurities like carbon, facilitating the subsequent separation of the active material from the Al foil [23]. The dried cathode material was then placed in deionized water (at room temperature) to peel the active material from the Al foil. The separated active material was collected and dried at 60 °C overnight. Subsequently, agate balls and the cathode material sheets were mixed at a mass ratio of 3:1 in a ball mill at room temperature. A mixture of medium and small zirconia grinding balls (D80 = 10 mm) was used as the grinding media. The

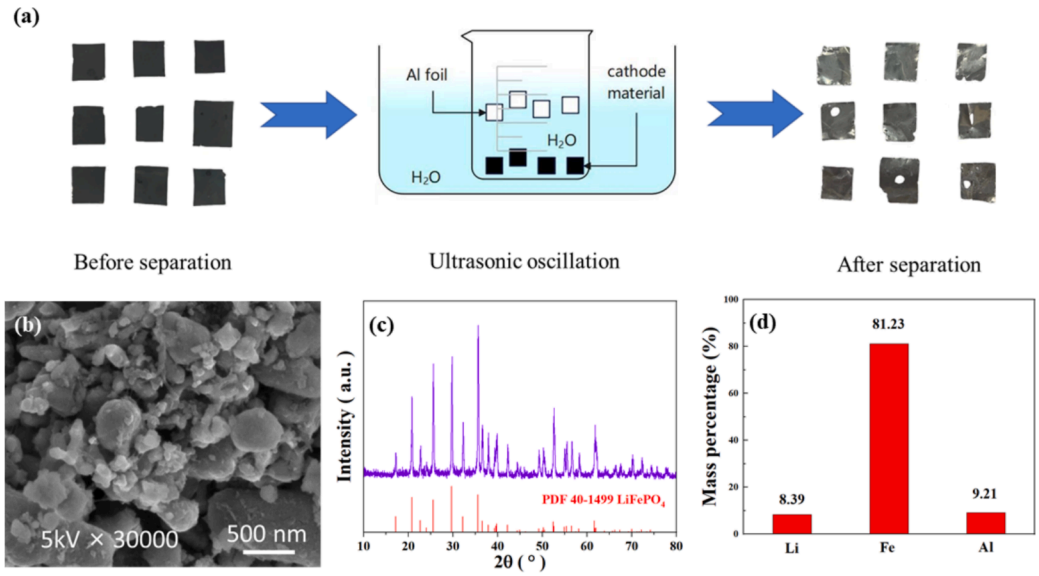

Fig. 1. (a) Schematic diagram of the ultrasonic separation of aluminum foil and cathode material. (b) SEM image of the cathode powder. (c) XRD pattern of the cathode powder. (d) The mass percentage of each metal element in the cathode material.

mixture underwent mechanical activation at different speeds and durations, with the forward and reverse rotation intervals set at 5 min to prevent heat accumulation. Finally, the powder was analyzed using XRD, a laser particle size analyzer, and FE-SEM.

2.4. Chemical element analysis

A microwave digestion system was used to digest the cathode material powder for its chemical element analysis. Typically, 0.1 g of cathode material powder is digested using 9–10 mL of aqua regia at 185° C and 2.5 MPa pressure. After filtration, the solution was used for measurement by inductively coupled plasma optical emission spectrometry (ICP-OES).

2.5. Batch leaching procedure

The batch leaching of raw material powder was conducted in 25-mL beakers. Typically, H_3PO_4 or H_3PO_4-H_2O_2 solution was used to leach raw material powder at different temperatures and reaction time ranges. After the leaching process, the solid residues were filtered using a sintered glass funnel. The solid residues were washed 3–5 times with deionized water and then dried at 60 °C for 12 h. The leachate was diluted and filtered using a syringe filter with a pore size of 0.22 μm for ICP testing. The effects of the phosphoric acid concentration, solid–liquid ratio, amount of hydrogen peroxide added, and temperature on the leaching rate were investigated.

The leaching rate of metal ions was calculated using Eq. (1),

$$L_x = \frac{C_x \bullet V_x}{m \bullet \omega_x} \tag{1}$$

where C_x (g/L) and V (L) represent the concentration of element "x" and the volume of the filtrate, respectively. And m (g) and ω_x denote the mass of the cathode active material and the weight content of element "x" in the initial active material.

2.6. Li recovery

The Li-rich leachate was recovered in the form of Li_2CO_3 by adding sodium carbonate. Firstly, 15 g of Na_2CO_3 powder was added to 50 mL of deionized water to prepare a saturated sodium carbonate solution. To increase the Li concentration, the leachate was evaporated at 70 °C by heating, while NaOH was added to adjust the pH value to 8–9 [19]. Finally, the saturated sodium carbonate solution was added dropwise to the leachate at 95 °C, resulting in the formation of a white powder. The powder was filtered using a Buchner funnel and washed with deionized water, and then dried at 60 °C for 24–48 h.

2.7. $FePO_4$ separation and recovery

In this study, the leaching residue contained Al impurities mixed with iron phosphate. A magnetic separation procedure was used for the recovery of iron phosphate. A total of 5 g of the dried leaching residue was placed in a 25-mL glass beaker, and a magnet was then placed externally to separate the $FePO_4$ from the residue mixture, repeating this step several times. The $FePO_4$ powder was finally collected and dissolved in acid for ICP testing to determine the purity and recovery rate.

The recovery rate (θ) of $FePO_4$ was calculated using Eq. (2),

$$\theta = \frac{m_x \bullet p_x \bullet M_F}{m_0} \tag{2}$$

Where m_x and p_x represents the mass and the purity of the final product after x rounds of magnetic separation, M_F refers to the molar mass proportion of Fe in $FePO_4$, and m_0 is the mass of Fe in the raw active material as tested by ICP.

3. Results and discussion

3.1. Physical separation and characterizations

In this study, an optimized environmentally friendly water stripping method was utilized based on our previous published methods [19]. To remove organic binders such as PVDF and impurities like carbon and facilitate faster separation of the cathode material from the Al foil, the sheets were cut into 10 × 10 mm pieces, calcinated at 450 °C for 120 min. After cooling, the sheets were immersed in deionized water, assisting the separation with ultrasonic agitation (Fig. 1a). The separation time was tested, and complete stripping of the cathode active material from the Al was achieved in ~ 30 s, which is faster than the reported ~ 70 s in our previously published laboratory study [20]. Throughout the entire stripping process, an aluminum stripping efficiency of 93.7 wt% was achieved, indicating that a portion of Al impurities had migrated into the active material powder. The residual Al,

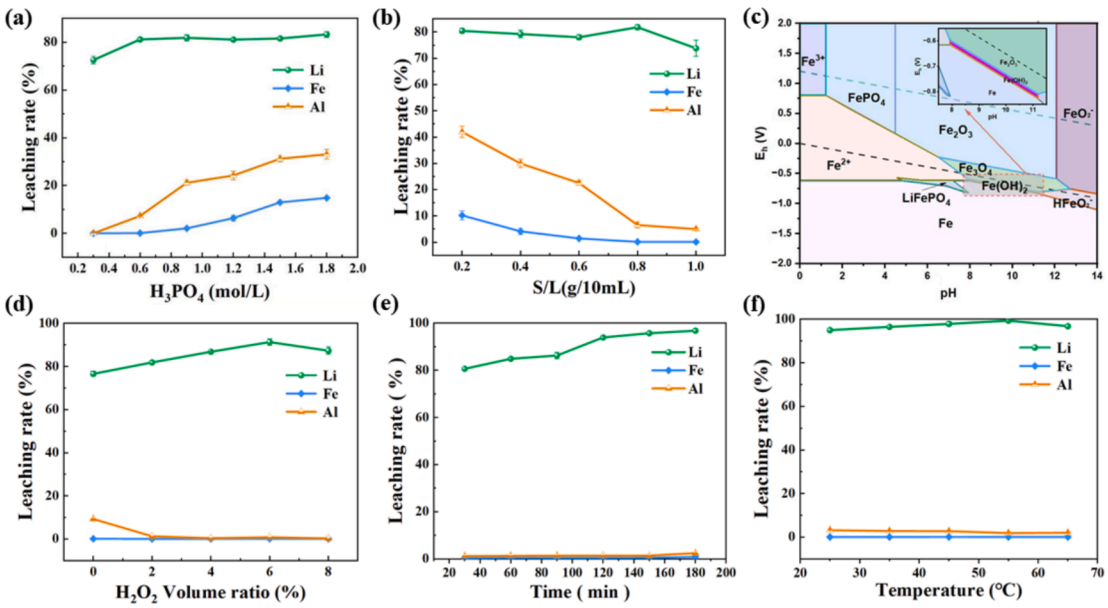

Fig. 2. The effect of leaching conditions on the leaching rates of Li, Fe, and Al. (a) Effect of the phosphoric acid concentration (S/L = 0.8 g/10 mL; 25 °C; 120 min; without H_2O_2). (b) Effect of the S/L ratio (0.6 M H_3PO_4; 25 °C; 120 min; without H_2O_2). (c) Eh–pH diagram for the Li–Fe–P–H_2O system at 298.15 K (data were obtained from HSC Chemistry 6.0 software). (d) Effect of the H_2O_2 content (0.6 M H_3PO_4; S/L = 0.8 g/10 mL; 25 °C; 120 min). (e) Effect of leaching time (0.6 M H_3PO_4; S/L = 0.8 g/10 mL; 6 vol% H_2O_2; 25 ℃), (f) Effect of leaching temperature (0.6 M H_3PO_4; S/L = 0.8 g/10 mL; 6 vol% H_2O_2; 120 min).

which is difficult to strip, will be removed through selective leaching, with over 99 wt% ultimately recovered as solid Al_2O_3. The obtained cathode active material was ground into fine powder, and SEM imaging of cathode active material revealed some degree of obvious agglomeration Fig. 1b, which is in line with previously published SEM images [20]. The structure of the ground powder was identified from the XRD pattern, as presented in Fig. 1c. The active material powder displayed a good match with the standard PDF card no. 40–1499 for $LiFePO_4$. The composition of active material powder was analyzed by ICP-OES in its digestion solution, and the metal elemental contents (wt%) of the cathode active powder were 8.39 wt% Li, 81.23 wt% Fe, 0 wt% F and 9.21 wt% Al (Fig. 1d), The three elements Li, Fe, and Al account for nearly 100 % of the total mass, demonstrating the effective removal of impurities such as PVDF and carbon.

3.2. Selective leaching of Li

3.2.1. Effect of phosphoric acid concentration

The effect of different concentrations of phosphoric acid on the metal leaching rates was examined, with the phosphoric acid concentration ranging from 0.3 to 1.8 mol/L (Fig. 2a). When the concentration of phosphoric acid was increased from 0.3 to 0.6 M, the leaching rate of Li increased from 71.52 % to 80.63 %, while the leaching rate of Fe displayed a slight increase from 0 % to 0.2 %, and the leaching rate of Al increased from 0 % to 7.05 %. When the phosphoric acid concentration was further increased to 1.8 M, the leaching rate of Li remained almost constant, while the leaching rates of Fe and Al increased to 13.44 % and 31.28 %, respectively. Based on the above results, the phosphoric acid concentration has a positive effect on the leaching of all metal ions, but Li leaching does not significantly increase when the phosphoric acid concentration is raised beyond 0.6 M. The possible reason for this may be related to the thermodynamic effects of the leaching reaction of $LiFePO_4$. In this solution, phosphoric acid maintains a certain ionization equilibrium in aqueous solution, and under this equilibrium, continuously adding more phosphoric acid may not significantly enhance the activity and concentration of H^+ [17]. To minimize the leaching of Fe and Al impurities, 0.6 mol/L of H_3PO_4 acid was chosen for the following experiments.

3.2.2. Effect of solid–liquid ratio

The solid–liquid (S/L) ratio is one important testing factors for the leaching rate of metals. In this study, The S/L ratio was varied from 0.2 to 1.0 g/10 mL with other conditions kept constant (Fig. 2b). The leaching rate of Li decreased slightly between 0.2–0.6 g/10 mL. The maximum leaching of Li was observed at 0.8 g/10 mL, with the leaching rate being 81.32 %. Conversely, the leaching rate of Fe decreased from 11.7 % to 0.5 % and that of Al decreased from 42.66 % to 7.2 % at 0.8 g/10 mL, and then remained relatively stable. By appropriately increasing the S/L ratio, ensuring that the amount of solid phase remains within the leaching capacity of the acid and the recovery rate of Li can be increased. Thus, an S/L ratio of 0.8 g/10 mL was selected for the subsequent experiments.

3.2.3. Effect of H_2O_2 amount

To better understand the leaching efficiency, an Eh–pH diagram for the Li–Fe–P–H_2O system at 298.15 K was produced by using HSC Chemistry 6.0 software (Fig. 2c) [18,19]. Based on the E_h–pH diagram, it can be observed that increasing the oxidation potential can achieve a higher conversion of $LiFePO_4$ to $FePO_4$, with the intermediate state being the ionic form of divalent Fe. This demonstrates that this method requires disruption of the spatial structure of $LiFePO_4$ and an increase in the oxidation potential to achieve the desired transformation. Thus, the addition of H_2O_2 can promote the conversion of Fe from divalent to trivalent, forming iron phosphate in situ, which facilitates the release of Li and enables the separation of Li and Fe [18]. In this experiment, we explored the optimal relative proportions of H_3PO_4 and H_2O_2 by adjusting the amount of H_2O_2. The impact of different H_2O_2 contents on the leaching rates of metal ions is illustrated in Fig. 2d. It can be observed that with an increase in the amount of H_2O_2, the leaching rate of Li continuously increases, reaching a maximum of 91.42 % at 6 vol% H_2O_2, and thereafter begins to decrease. The possible reason for this is that excessive H_2O_2 can oxidize divalent iron to trivalent iron and hydrolyze to produce iron hydroxide colloids that cover and wrap around the material surface, hindering the release of Li and reducing its leaching rate However, the leaching rates of Fe and Al continuously decrease to nearly 0 % and remain stable thereafter. This indicates that the addition of H_2O_2 not only enhances the leaching rate of Li but also aids in the

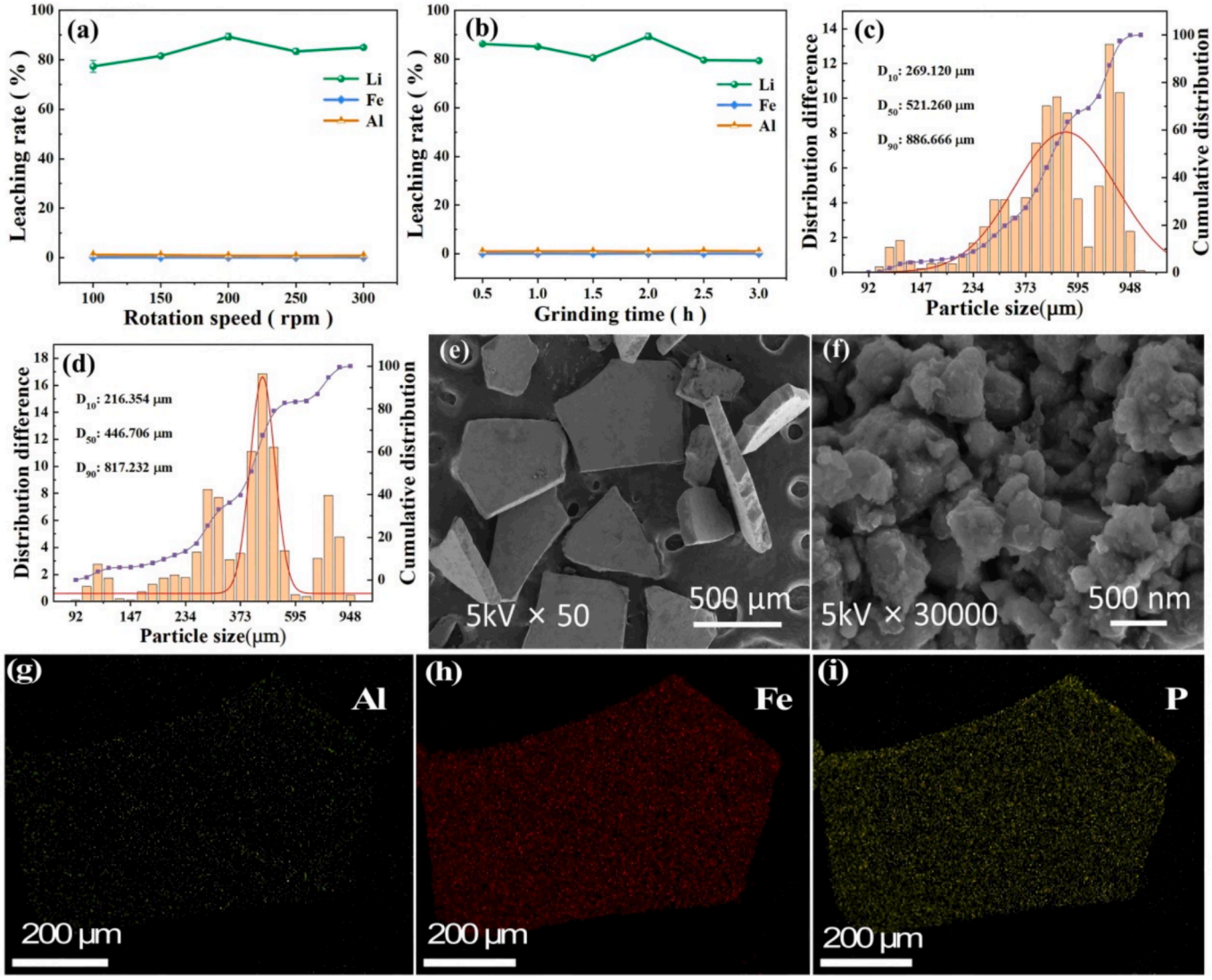

Fig. 3. (a) Effect of rotation speed (grinding time = 2 h). (b) Effect of grinding time (rotation speed = 200 rpm). The particle size distribution after (c) 1 h, (d) 2 h. (e–f) SEM images of the powders under the optimal ball milling conditions. (g–i) Element distributions for Al, Fe and P.

removal of Fe and Al impurities.

3.2.4. *Effect of leaching time*

To investigate the progress of the leaching reaction over time, this study examined the effect of leaching time under the optimized reaction conditions determined in the previous experiments (phosphoric acid concentration of 0.6 M, S/L ratio of 0.8 g/10 mL, H_2O_2 concentration of 6 vol%, and room temperature). The leaching time ranged between 30 and 180 min, as shown in Fig. 2e. After 30 min of reaction, the leaching rate of Li reached 81.3 %, while the leaching rates of Fe and Al were nearly zero. By 120 min, the Li leaching rate exceeded 93 %, with Fe and Al leaching rates displaying minimal changes and remaining close to zero. When the reaction time was extended to 180 min, the increase in the Li leaching rate slowed and stabilized, with an increase of less than 2 %, while the Al leaching rate began to rise to around 3 %. Through linear regression analysis of the leaching time-kinetics data, it was found that the overall linear trend before 120 min aligns more closely with the first-order reaction kinetics model: $\ln(1 - L_{Li}) = -kt$. The calculated equation is $\ln(1 - L_{Li}) = -0.0145\,t - 1.21$, with a correlation coefficient $R^2 = 0.952$. However, after 120 min, a significant deviation occurs. Fitting analysis revealed better agreement with the diffusion-controlled mechanism (shrinking core model), yielding the equation $(1)-(1 - L_{Li})^{1/3} = 0.0038\,t + 0.332$, with a correlation coefficient $R^2 = 0.985$. In conclusion, the leaching process conforms to a two-stage mixed control model: during the initial reaction stage (<90 min), it is controlled by chemical reactions, while in the middle and late stages (≥90 min), it is governed by the shrinking core model. Considering factors such as energy efficiency and metal separation purity, 120 min was selected as the optimal leaching reaction time.

3.2.5. *Effect of leaching temperature*

The reaction temperature plays a crucial role in influencing the outcomes of thermodynamically driven processes, such as leaching reactions. The leaching experiments on $LiFePO_4$ active material were conducted at different temperatures ranging from 25 °C to 65 °C, and the results are presented in Fig. 2f. As the temperature increased, the leaching rate of Li continuously increased, reaching a maximum of 99.5 % at 55 °C. At this temperature, the leaching rates of Fe and Al slightly decreased, with values of 0.424 % and 1.824 %, respectively. However, when the temperature was further increased to 65 °C, the leaching rate of Li decreased. This is because during the leaching process, H_3PO_4 reacts with $LiFePO_4$, breaking down and dissolving the Li^+ components. This leaching reaction requires energy to break the bonds in $LiFePO_4$, and it is therefore generally characterized as an endothermic reaction.

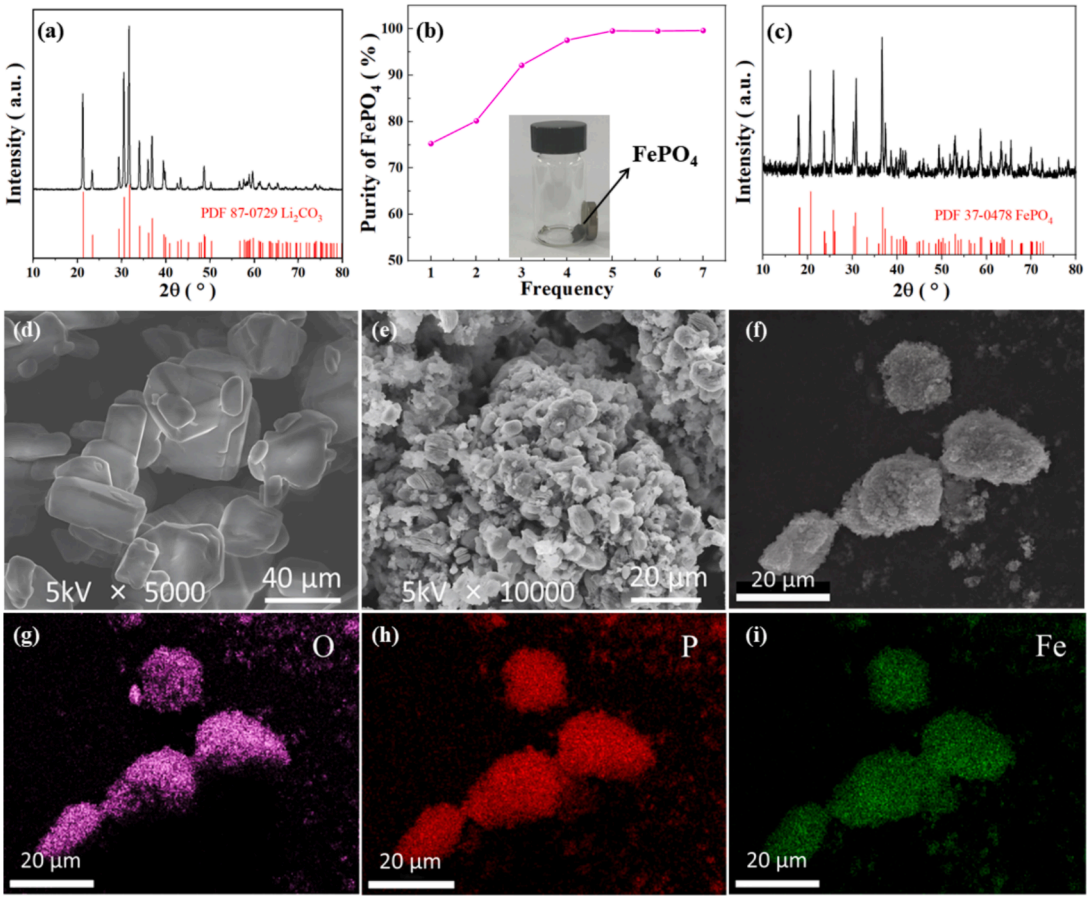

Fig. 4. (a) XRD pattern of Li_2CO_3. (b) Effect of magnetic separation time on the purity of $FePO_4$. (c) XRD pattern of $FePO_4$. SEM images of (d) Li_2CO_3 precipitate and (e–f) $FePO_4$. (g–i) Element distributions of $FePO_4$.

Moreover, during this reaction, acid interacts with the solid material through ion exchange or dissolution, where energy is typically consumed to facilitate the leaching of Li. Additionally, due to the ionization equilibrium of phosphoric acid, as the acid concentration increases, the activity of H^+ and the leaching efficiency may not improve significantly, further supporting the notion that this process is endothermic. However, when the temperature further increased to 65 ℃, the leaching rate of Li slightly decreased, which may be due to the high temperature affecting the stability of H_2O_2. Therefore, 55 °C was chosen as the optimal leaching temperature.

3.3. *Effect of mechanical activation*

In our previous study, the particle size of active materials significantly influenced the leaching efficiency in the H_2SO_4–H_2O_2 system [16]. In this study, the optimal leaching efficiency in relation to particle size was achieved by optimizing the speed and duration of mechanical activation. The effect of milling speed on the leaching rates of various metals is illustrated in Fig. 3a, with the ball-to-powder ratio (BPR) set at 3 and the milling time maintained at 2 h. As the speed increased, the leaching rate of Li initially rose continuously, reaching a peak at 200 rpm before slightly decreasing. The leaching rates of Fe and Al remained near zero. This phenomenon can be attributed to the possibility that excessive speed may cause powder agglomeration and adhesion, leading to a reduction in the leaching rate. Therefore, 200 rpm was chosen as the optimal rotation speed for mechanical activation.

Fig. 3b illustrates the effect of milling time on the leaching rates of various metals when the BPR was 3 and the rotation speed was 200 rpm. The leaching rate of Li initially slowly increased as the ball milling time increased, reaching its highest rate at 2 h. In addition, the leaching rates of Fe and Al remained close to zero. Finally, 2 h was selected as the optimal milling time at the rotation speed of 200 rpm. In summary, it can be observed that mechanical activation indeed exerts a positive effect on lithium leaching, primarily due to mechanical forces inducing the cleavage of chemical bonds, the generation of unsaturated groups, free ions, and electrons, as well as the formation of reactive surfaces. These processes are accompanied by the creation of lattice defects and an increase in internal energy under ambient pressure and temperature conditions.

To reveal the influence of ball milling conditions on the Li leaching rate, the particle size of $LiFePO_4$ cathode material powders under different ball milling conditions was determined. As presented in Fig. 3c–d, in the mechanical activation speed test, 200 rpm yielded the highest Li leaching efficiency of 84.25 % with good selectivity, achieving a particle size D50 of 521.26 μm after 1 h. After optimization, extending the grinding to 2 h at 200 rpm increased the Li leaching efficiency to 90.16 % with good selectivity, and reduced the particle size D50 to 446.706 μm. However, as shown in the particle size distributions under different conditions Fig. S1–S2, further reductions in particle size (D50 313.653 μm after 2.5 h and 303.603 μm after 3 h of grinding at 200 rpm) did not significantly improve the leaching efficiency.

After consideration of the leaching results and the energy consumption, milling of cathode material powders under conditions of 200 rpm for 2 h was chosen for the selected optimal operation conditions. Additionally, SEM images of the powders obtained under these conditions Fig. 3e–f revealed ~ 400 μm particles with nanoscale fine particles assembled on the surfaces. The corresponding SEM-EDS mapping of elemental distribution Fig. 3g–i demonstrates the uniform distribution of Al, Fe, and P, with a significantly lower Al content compared to Fe and P. This result is consistent with the previous ICP test results.

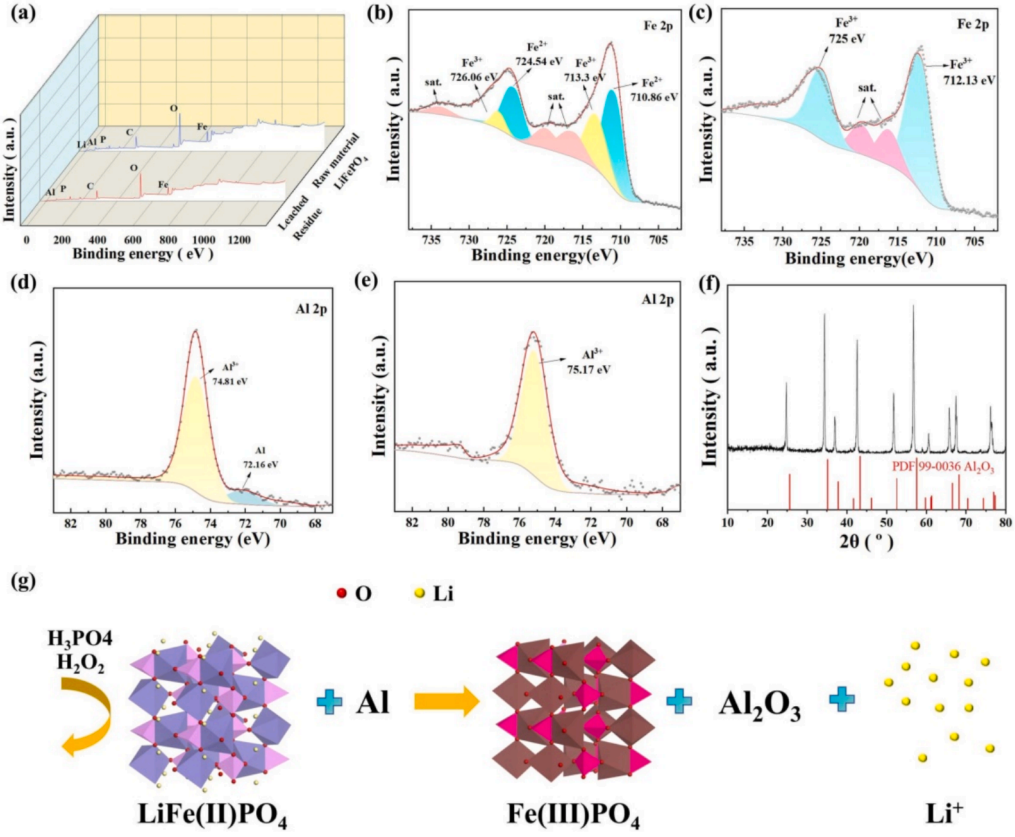

Fig. 5. (a) Full XPS spectrum of spent LFP cathode powder and leached residue; (b–c) XPS spectrum of Fe2p from spent LFP cathode materials after milling at a speed of 200 rpm for 2 h and leached residue from the H_3PO_4–H_2O_2 leaching system. (d–e) XPS spectrum of Al2p from spent LFP cathode materials after milling at a speed of 200 rpm for 2 h and leached residue from the H_3PO_4–H_2O_2 leaching system. (f) The XRD pattern of leaching Al residue after magnet separation. (g) The proposed mechanism of the H_3PO_4-H_2O_2 leaching system for the obtained active black materials.

3.4. Recovery of Li and $FePO_4$

The Li-rich leachate was recovered as a Li_2CO_3 precipitate by adding sodium carbonate as a precipitating agent. The leachate obtained under the optimized conditions was further concentrated through evaporation. The precipitation temperature for Li_2CO_3 was set at 95 °C, as the solubility of Li_2CO_3 in water decreases with increasing temperature. XRD testing of the precipitated Li_2CO_3, as illustrated in Fig. 4a, exhibited peak patterns that closely match the standard PDF card for lithium carbonate, indicating successful precipitation of Li_2CO_3. According to the ICP test results, the purity of the precipitated lithium carbonate was 99.2 %.

Magnetic separation was utilized to remove Al impurities, as $FePO_4$ exhibits certain magnetic properties, while Al impurities do not. However, due to the friction and adhesion between the powder particles, complete separation cannot be achieved in a single process. Thus, a multi-stage magnetic separation method was used to separate $FePO_4$ from Al impurities, with the results presented in Fig. 4b. After each magnetic separation, a purity test was conducted. The relationship between the number of magnetic separations and the purity of $FePO_4$ is illustrated in Fig. 4b. After five magnetic separations, the purity of $FePO_4$ reached 98.5 %, and it further increased after six and seven magnetic separations, with the purity of $FePO_4$ being maintained at over 99 %. Furthermore, the recovery rate of $FePO_4$ was calculated to be 97.6 %. Fig. 4c presents the XRD pattern of $FePO_4$ recovered by this process. It can be observed that the pattern matches well with the PDF standard card of $FePO_4$, and no other impurity peaks were observed.

Fig. 4d presents an SEM image of Li_2CO_3, which displays some degree of agglomeration. The SEM images of $FePO_4$ are displayed in Fig. 4e–f, in which noticeable agglomeration can be observed. EDS analysis Fig. 4g–i revealed the presence of the elements O, P, and Fe, all exhibiting a very uniform distribution. Additionally, no Al or other impurity elements were detected.

3.5. Mechanism analysis

To investigate the mechanism in the entire reaction, XPS tests were conducted on the active material powder before and after leaching. Fig. 5a presents the full XPS spectra analysis of the raw material and the leaching residue by H_3PO_4 acid leaching and the H_3PO_4–H_2O_2 leaching system. Peaks of elements such as Li, Al, Fe, P, C, and O were identified in the raw material, whereas only the Li peak disappeared in the leaching residue, indicating the selectivity of the leaching process for Li. Fig. 5b illustrates that the broader Fe peak in the raw material is mainly composed of $Fe2p_{1/2}$ and $Fe2p_{3/2}$ peaks at binding energies of 724.6 eV and 711 eV, respectively. The deconvolution of the $Fe2p_{3/2}$ peak reveals peaks at 710.86 eV and 713.3 eV, corresponding to Fe^{2+} and Fe^{3+}, respectively. Similarly, the $Fe2p_{1/2}$ peaks at 724.54 eV and 726.06 eV represent Fe^{2+} and Fe^{3+}, respectively. Additionally, two satellite peaks around 720 eV and 735 eV indicate the coexistence of Fe^{2+} and Fe^{3+}. Fig. 5c presents the Fe2p spectrum of the leaching residue, in which only the corresponding Fe^{3+} peaks are present in both $Fe2p_{1/2}$ and $Fe2p_{3/2}$, indicating a valence change of Fe during the leaching process. This observation is consistent with the XRD results for the recovered $FePO_4$ (Fig. 4c), with Fe valence 3 and no other impurities detected.

XPS fine spectra of Al before and after leaching were also analyzed, as presented in Fig. 5d–e. Before leaching, Al existed in both metal form (Al) and oxidized states (Al^{3+}), possibly due to partial oxidation of the Al foil used as the current collector. After leaching, only the oxidized state of Al remained, indicating that Al impurities did not form ionic Al^{3+}

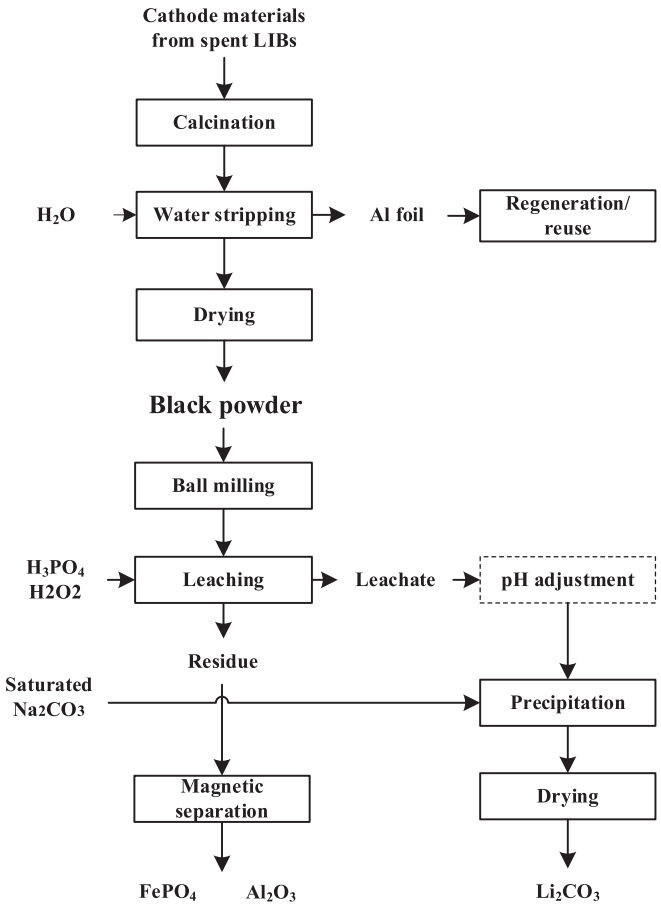

Fig. 6. The flowsheet of the developed green recycling process of cathode materials from spent LIBs.

through reaction with H^+ but instead formed Al_2O_3 in situ under the action of H_2O_2. This interpretation was validated by the XRD pattern of the Al residue following magnetic separation from $FePO_4$, which had undergone treatment in the H_3PO_4-H_2O_2 leaching process. As shown in Fig. 5f, the obtained XRD results align well with the standard PDF card for Al_2O_3. The H_3PO_4-H_2O_2 leaching process may be related to the Fenton reaction, where under the action of H_2O_2, part of it acts on the intact olivine structure of $LiFePO_4$, converting it in situ into $FePO_4$ with the same spatial structure. Another part reacts with free Fe^{2+} in a heterogeneous Fenton-like reaction, generating ·OH radicals that promote the transformation of LFP to $FePO_4$ [26]. During this process, the overall reaction, as shown in Eq. (3)–(4), continuously transforms Fe(II) into Fe (III), and this process is accompanied by the release of Li^+, which is a crucial factor in achieving the separation of Li and Fe.

$$LiFePO_4 + H_2O_2 \rightarrow Li^+ + FePO_4 + OH^- + \bullet OH \quad (3)$$

$$Fe^{2+} + \bullet OH + PO_4^{3-} \rightarrow FePO_4 + OH^- \quad (4)$$

This process allowed a large amount of H^+ to replace Li, promoting the release of Li from the $LiFePO_4$ olivine structure. This explains why the addition of hydrogen peroxide enhanced the leaching of Li.

The Li leaching process during the reaction is illustrated in the accompanying diagram (Fig. 5g). Under the combined action of phosphoric acid and hydrogen peroxide, Li is extracted from the spatial framework formed by FeO_6 octahedra and PO_4 tetrahedra. This process involves the deintercalation of Li into free Li^+ ions.

Table 1
Experimental inputs, energy consumption and waste products from one batch (one batch for 1.0 kg LIBs).

Materials	Flow per batch	Cost/ US$ per ton (Market price in China in 2024)	Cost/ US$ per batch
Water (L)	12.5	0.59	0.01
H_3PO_4 (L)	0.214	1,250	0.26
H_2O_2 (L)	0.1	700	0.07
Na_2CO_3 (kg)	0.264	1,680	0.44
Waste LIBs (kg)	1.0	1,330	1.33
Electricity	–	0.15/kWh	0.48
Calcination	0.088		
Stripping	0.15		
Drying	0.066		
Ball milling	0.82		
Leaching	0.66		
Filtration	0.09		
Magnetic separation	0.74		
Precipitation/ drying	0.66		
Total			2.59

Table 2
Cost and net products value for one batch experiment.

Categories	Cost/ US$
Chemicals and waste LIBs, etc.	2.11
Electricity	0.48
Landfilling as hazardous waste	−0.37
Products value (Li_2CO_3, $FePO_4$)	−5.31

3.6. Process economic assessment

Based on the experimental results presented in Fig. 6 and the data from the literature (Table 1), material turnover and energy consumption were calculated and evaluated. A preliminary assessment of the process cost was conducted. The expense for a single batch experiment (1 kg of waste LIBs treatment) is approximately $2.59 (Table 1), while the value of the products (Li_2CO_3, $FePO_4$) contributes significantly to the profit, totaling $5.31 (Table 2). The value of the products easily offsets the costs associated with chemicals and electricity. Furthermore, the overall process cost could be further reduced when scaled up to an industrial level. Comparing the expense and profit, it is evident that our process consumes fewer chemicals and energy while achieving a higher-purity Li_2CO_3 and $FePO_4$ product. This optimized strategy demonstrates significant potential for the efficient recovery of LIBs. For future work, a comprehensive evaluation of both the economic and environmental aspects, including labor costs, maintenance, CO_2 emission and secondary waste treatment, is recommended, particularly at a laboratory pilot scale.

4. Conclusions

In this study, a green and efficient selective recovery process was developed and optimized for the recycling of $LiFePO_4$ batteries. During the pretreatment stage, an environmentally friendly water stripping method was used to successfully separate the damaged Al foil from the cathode active material. In subsequent work, the optimal leaching conditions were determined through the adjustment of leaching parameters: 0.6 mol/L H_3PO_4, S/L ratio of 0.8 g/10 mL, 6 vol% H_2O_2, at a temperature of 55 °C, with the active material subjected to ball milling at 200 rpm for 2 h. Under these conditions, 99.5 % of Li was successfully leached, while Fe and Al impurities remained in the solid phase. Sodium carbonate was used as a precipitating agent to convert Li_3PO_4 to Li_2CO_3, achieving a purity of over 98 %. A convenient and environmentally friendly magnetic separation method was designed to separate $FePO_4$

from Al impurities. After seven cycles of magnetic separation, the purity and the recovery rate of $FePO_4$ reached 99 % and 97.6 %, respectively. Additionally, the leaching mechanism revealed the oxidation behavior of $LiFePO_4$ under the given process conditions, forming $FePO_4$ with an olivine structure. The dual action of H^+ replacement and the Fenton reaction with H_2O_2 facilitated the release of Li, while Al remained in the solid phase as an oxide for separation. This study demonstrates practical significance in the recovery of $LiFePO_4$ with Al impurities and emphasizes the environmental friendliness and efficiency of the process, and A preliminary economic assessment of the developed recycling process indicates considerable promise for industrial application, showing great potential for addressing a series of related issues in the recycling of lithium iron phosphate batteries.

CRediT authorship contribution statement

Shengxiao Niu: Data curation, Software, Writing – original draft. **Puwu Liang:** Methodology, Formal analysis, Writing – review & editing. **Zhicheng Zhang:** Writing – review & editing. **Jinfeng Tang:** Methodology, Writing – review & editing. **Minhua Su:** Investigation, Writing – review & editing. **Hongli Bao:** Investigation, Writing – review & editing. **Junhua Xu:** Conceptualization, Funding acquisition, Methodology, Supervision, Writing – original draft, Writing – review & editing.

Declaration of competing interest

The authors declare that they have no known competing financial interests or personal relationships that could have appeared to influence the work reported in this paper.

Acknowledgements

The research leading to these results received funding from the Chinese Academy of Sciences Pioneer “Hundred Talents Program” Young Talents (Class C). This publication reflects only the authors’ views, exempting the Community from any liability.

Appendix A. Supplementary data

Supplementary data to this article can be found online at https://doi.org/10.1016/j.seppur.2025.133350.

Data availability

Data will be made available on request.

References

[1] J. Rogelj, O. Geden, A. Cowie, A. Reisinger, Net-zero emissions targets are vague: three ways to fix, Nature 591 (2021) 365–368, https://doi.org/10.1038/d41586-021-00662-3.
[2] X. He, F. Tian, H. Song, C. Wang, Room temperature reversible Ca-metal chemistry in commercial fluorinated calcium salt ester electrolytes enabled by a compact N-rich interphase layer, Chem. Eng. J. 502 (2024) 157793, https://doi.org/10.1016/j.cej.2024.157793.
[3] K. He, Z.-Y. Zhang, L. Alai, F.-S. Zhang, A green process for exfoliating electrode materials and simultaneously extracting electrolyte from spent lithium-ion batteries, J. Hazard. Mater. 375 (2019) 43–51, https://doi.org/10.1016/j.jhazmat.2019.03.120.
[4] S. Wang, Y. Lai, J. Yang, J. Zhao, Y. Zhang, M. Chen, J. Tang, J. Xu, M. Su, Advances in Recycling Technologies of Critical Metals and Resources from Cathodes and Anodes in Spent Lithium-Ion Batteries, Separations. 12 (2025) 4, https://doi.org/10.3390/separations12010004.
[5] X. Zhong, J. Han, L. Chen, W. Liu, F. Jiao, H. Zhu, W. Qin, Binding mechanisms of PVDF in lithium ion batteries, Appl. Surf. Sci. 553 (2021) 149564, https://doi.org/10.1016/j.apsusc.2021.149564.
[6] E. Markevich, G. Salitra, D. Aurbach, Influence of the PVDF binder on the stability of $LiCoO_2$ electrodes, Electrochem. Commun. 7 (2005) 1298–1304, https://doi.org/10.1016/j.elecom.2005.09.010.
[7] W. Guo, D. Fu, F. Tian, H. Song, C. Wang, Ca-based hybrid interfaces inhibit uncontrolled electrolyte decomposition for efficient ion-storage, Chem. Eng. J. 489 (2024) 151116, https://doi.org/10.1016/j.cej.2024.151116.
[8] T. Kwon, Y.K. Jeong, E. Deniz, S.Y. AlQaradawi, J.W. Choi, A. Coskun, Dynamic cross-linking of polymeric binders based on host–guest interactions for silicon anodes in lithium ion batteries, ACS Nano 9 (2015) 11317–11324, https://doi.org/10.1021/acsnano.5b05030.
[9] J.-C.-Y. Jung, P.-C. Sui, J. Zhang, A review of recycling spent lithium-ion battery cathode materials using hydrometallurgical treatments, J. Energy Storage 35 (2021) 102217, https://doi.org/10.1016/j.est.2020.102217.
[10] O. Kwon, I. Sohn, Fundamental thermokinetic study of a sustainable lithium-ion battery pyrometallurgical recycling process, Resour. Conserv. Recycl. 158 (2020) 104809, https://doi.org/10.1016/j.resconrec.2020.104809.
[11] M. Wang, K. Liu, S. Dutta, D.S. Alessi, J. Rinklebe, Y.S. Ok, D.C.W. Tsang, Recycling of lithium iron phosphate batteries: Status, technologies, challenges, and prospects, Renew. Sustain. Energy Rev. 163 (2022) 112515, https://doi.org/10.1016/j.rser.2022.112515.
[12] Y. Dai, Z. Xu, D. Hua, H. Gu, N. Wang, Theoretical-molar Fe^{3+} recovering lithium from spent $LiFePO_4$ batteries: An acid-free, efficient, and selective process, J. Hazard. Mater. 396 (2020) 122707, https://doi.org/10.1016/j.jhazmat.2020.122707.
[13] Beijing Institute of Technology, L. Li, J. Lu, Argonne National Laboratory, L. Zhai, Beijing Institute of Technology, X. Zhang, Beijing Institute of Technology, L. Curtiss, Argonne National Laboratory, Y. Jin, China Electric Power Research Institute, F. Wu, Beijing Institute of Technology, R. Chen, Beijing Institute of Technology, K. Amine, Argonne National Laboratory, A facile recovery process for cathodes from spent lithium iron phosphate batteries by using oxalic acid, CSEE J. Power Energy Syst. 4 (2018) 219–225. doi: 10.17775/CSEEJPES.2016.01880.
[14] P. Yadav, C.J. Jie, S. Tan, M. Srinivasan, Recycling of cathode from spent lithium iron phosphate batteries, J. Hazard. Mater. 399 (2020) 123068, https://doi.org/10.1016/j.jhazmat.2020.123068.
[15] Y. Song, B. Xie, S. Song, S. Lei, W. Sun, R. Xu, Y. Yang, Regeneration of $LiFePO_4$ from spent lithium-ion batteries via a facile process featuring acid leaching and hydrothermal synthesis, Green Chem. 23 (2021) 3963–3971, https://doi.org/10.1039/D1GC00483B.
[16] W. Liu, K. Li, W. Wang, Y. Hu, Z. Ren, Z. Zhou, Selective leaching of lithium ions from $LiFePO_4$ powders using hydrochloric acid and sodium hypochlorite system, Can. J. Chem. Eng. 101 (2023) 1831–1841, https://doi.org/10.1002/cjce.24617.
[17] X. Chen, H. Ma, C. Luo, T. Zhou, Recovery of valuable metals from waste cathode materials of spent lithium-ion batteries using mild phosphoric acid, J. Hazard. Mater. 326 (2017) 77–86, https://doi.org/10.1016/j.jhazmat.2016.12.021.
[18] Y. Yang, X. Zheng, H. Cao, C. Zhao, X. Lin, P. Ning, Y. Zhang, W. Jin, Z. Sun, A closed-loop process for selective metal recovery from spent lithium iron phosphate batteries through mechanochemical activation, ACS Sustain. Chem. Eng. 5 (2017) 9972–9980, https://doi.org/10.1021/acssuschemeng.7b01914.
[19] Q. Jing, J. Zhang, Y. Liu, C. Yang, B. Ma, Y. Chen, C. Wang, E-pH diagrams for the Li-Fe-P-H_2O system from 298 to 473 K: Thermodynamic analysis and application to the wet chemical processes of the $LiFePO_4$ cathode material, J. Phys. Chem. C 123 (2019) 14207–14215, https://doi.org/10.1021/acs.jpcc.9b02074.
[20] Z. Zhang, J. Tang, M. Su, J. Xu, K. Shih, Design and optimization of an economically viable and highly efficient strategy for Li recycling from spent $LiFePO_4$ batteries, ACS Sustain. Chem. Eng. 11 (2023) 16124–16132, https://doi.org/10.1021/acssuschemeng.3c03797.
[21] G. Liu, Z. Liu, J. Gu, H. Yuan, Y. Wu, Y. Chen, A facile new process for the efficient conversion of spent $LiFePO_4$ batteries via $(NH_4)_2S_2O_8$-assisted mechanochemical activation coupled with water leaching, Chem. Eng. J. 471 (2023) 144265, https://doi.org/10.1016/j.cej.2023.144265.
[22] Y. He, X. Yuan, G. Zhang, H. Wang, T. Zhang, W. Xie, L. Li, A critical review of current technologies for the liberation of electrode materials from foils in the recycling process of spent lithium-ion batteries, Sci. Total Environ. 766 (2021) 142382, https://doi.org/10.1016/j.scitotenv.2020.142382.
[23] H. Bi, H. Zhu, L. Zhu, Y. Gao, S. Gao, J. Peng, H. Li, Low-temperature thermal pretreatment process for recycling inner core of spent lithium iron phosphate batteries, Waste Manage. Res. 39 (1) (2021) 146–155, https://doi.org/10.1177/0734242x20957403.
[24] R. Tao, P. Xing, H. Li, Z. Sun, Y. Wu, Recovery of spent $LiCoO_2$ lithium-ion battery via environmentally friendly pyrolysis and hydrometallurgical leaching, Resour. Conserv. Recycl. 176 (2022) 105921, https://doi.org/10.1016/j.resconrec.2021.105921.
[25] X. Chen, S. Li, X. Wu, T. Zhou, H. Ma, In-situ recycling of coating materials and Al foils from spent lithium ion batteries by ultrasonic-assisted acid scrubbing, J. Clean. Prod. 258 (2020) 120943, https://doi.org/10.1016/j.jclepro.2020.120943.
[26] K. Liu, J. Wang, M. Wang, Q. Zhang, Y. Cao, L. Huang, M. Valix, D.C.W. Tsang, Low-carbon recycling of spent lithium iron phosphate batteries via a hydro-oxygen repair route, Green Chem. 25 (2023) 6642–6651, https://doi.org/10.1039/D3GC00472D.